

## Supporting Information

### **Constructing 2D MOFs from 2D LDHs: highly efficient and durable electrocatalyst for water oxidation**

Mengke Cai,<sup>a</sup> Qinglin Liu,<sup>a</sup> Ziqian Xue,<sup>a</sup> Yinle Li,<sup>a</sup> Yanan Fan,<sup>a</sup> Aiping Huang,<sup>b</sup> Man-Rong Li,<sup>a</sup> Mark Croft,<sup>c</sup> Trevor A. Tyson,<sup>d</sup> Zhuofeng Ke<sup>e</sup> and Guangqin Li\*<sup>a</sup>

<sup>a</sup> MOE Laboratory of Bioinorganic and Synthetic Chemistry, Lehn Institute of Functional Materials, School of Chemistry, Sun Yat-Sen University, Guangzhou 510275, People's Republic of China. E-mail: [liguangqin@mail.sysu.edu.cn](mailto:liguangqin@mail.sysu.edu.cn)

<sup>b</sup> Key Laboratory of Polymer Composites and Functional Materials of Ministry of Education, School of Chemistry, Sun Yat-Sen University, Guangzhou 510275, People's Republic of China

<sup>c</sup> Department of Physics and Astronomy, Rutgers, The State University of New Jersey, 136 Frelinghuysen Road, Piscataway, New Jersey 08854, United States

<sup>d</sup> Department of Physics, New Jersey Institute of Technology, Newark, New Jersey 07102, United States

<sup>e</sup> Key Laboratory for Polymeric Composite and Functional Materials of Ministry of Education, School of Materials Science and Engineering, Sun Yat-Sen University, Guangzhou 510275, People's Republic of China

Number of pages: 20

Number of tables: 4

Number of Figures: 19

## EXPERIMENTAL SECTION

**Chemicals and Materials.** Sodium hydroxide (NaOH, AR95%), sodium carbonate ( $\text{Na}_2\text{CO}_3$ , AR98%), terephthalic acid (BDC, AR98%), cobalt(II) nitrate hexahydrate ( $\text{Co}(\text{NO}_3)_2 \cdot 6\text{H}_2\text{O}$ , AR98%), iron(III) nitrate nonahydrate ( $\text{Fe}(\text{NO}_3)_3 \cdot 9\text{H}_2\text{O}$ , AR98%), nafion solution (5%wt), *N,N*-dimethylformamide (DMF, AR99%) and ethanol (EtOH, AR99%) were purchased from Sigma-Aldrich and were used as received without further purification. Deionized water (resistivity  $> 18 \text{ M}\Omega \text{ cm}$ ) was used in all experiments from a Sartorius Arium comfort I system.

**Synthesis of precursor CoFe-LDH.** The CoFe-LDH nanosheets were prepared by hydrothermal method. 18 mmol  $\text{Co}(\text{NO}_3)_2 \cdot 6\text{H}_2\text{O}$  and 9 mmol  $\text{Fe}(\text{NO}_3)_3 \cdot 9\text{H}_2\text{O}$  were dissolved in 30 mL deionized water. 24 mmol  $\text{Na}_2\text{CO}_3$  and 57.6 mmol NaOH were dissolved in deionized water. Equal volumes of both solutions were added into beaker under vigorous stirring for 1 h, and transferred to a 100 mL-stainless-steel Teflon-lined autoclave and heated at 80 °C for 48 h. After natural cooled to room temperature, the resultant brown precipitates were separated from the reaction mixture by centrifugation, and washed thoroughly with deionized water and ethanol. Finally, the obtained solid was dried in vacuum at 60 °C for 12 h for further characterization and application.

**Synthesis of LM-*T-t* (*T*: temperature/°C, *t*: time/hour).** Typically, 50 mg CoFe-LDH was suspended in 30 mL DMF, and then the suspension was sonicated for 30 min. Subsequently, 100 mg BDC was added to the suspension, and the suspension was sonicated for another 30 min. Subsequently, the reaction mixture was transferred to a 50 mL stainless-steel Teflon-lined autoclave and heated at various temperature and time, with 5 degrees per minutes heating and natural cooling. The precipitate was isolated by centrifugation and washed with DMF and ethanol. The resultant material was dried in vacuum at 60 °C for 12 h for further characterization and application.

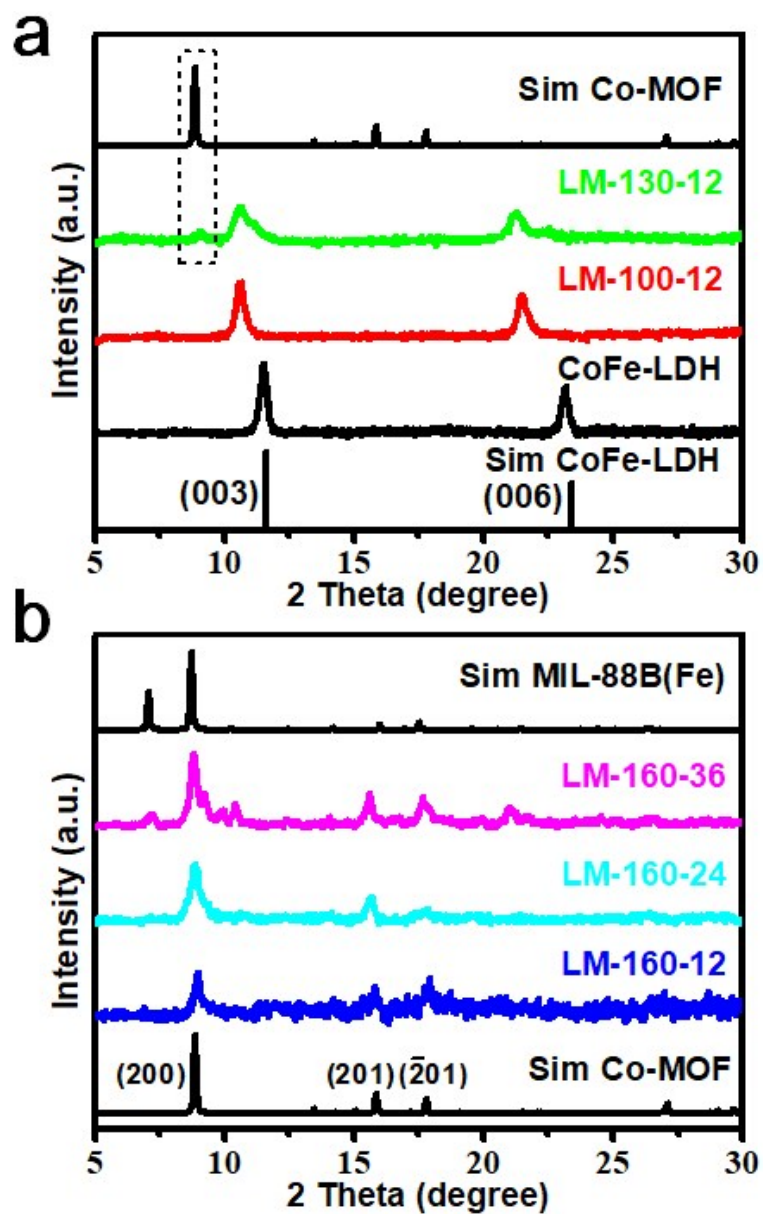
**Materials Characterizations.** Scan field-emission scanning electron microscopy (FESEM) images were performed on a Hitachi SU8010 scanning electron microscope

at 5.0 kV. Transmission electron microscopy (TEM) images were carried out using JEOL JEM-1400 at 120 kV. High angle annular dark field scanning transmission electron microscopy (HAADF-SEM) imaging and energy-dispersive X-ray spectroscopy (EDXS) elemental mapping were carried out on JEOL ARM200 at 300 kV. Powder X-ray diffraction (PXRD) patterns were recorded on a Rigaku SmartLab diffractometer with Cu K $\alpha$  ( $\lambda = 1.540598 \text{ \AA}$ ) radiation operating at 30 kV and 200 mA. X-ray photoelectron spectroscopy (XPS) was performed by a VG ESCALABMKII instrument. The content of Co and Fe in different specimens was determined by inductively coupled plasma-mass spectrometer (ICP-MS, Thermo Fisher Scientific). The N<sub>2</sub> adsorption-desorption isotherms were collected using a Quantachrome Instruments Autosorb-iQ2-MP at 77 K. The atomic force microscopy (AFM) was performed by a Bruker Multimode 8 instrument. X-ray absorption spectroscopy (XAS) at the Co and Fe K-edges was carried out at the QAS, 7-BM beamline at the National Synchrotron Light Source II at Brookhaven National Laboratory. The high performance liquid chromatography (HPLC) was conducted by Waters 1525.

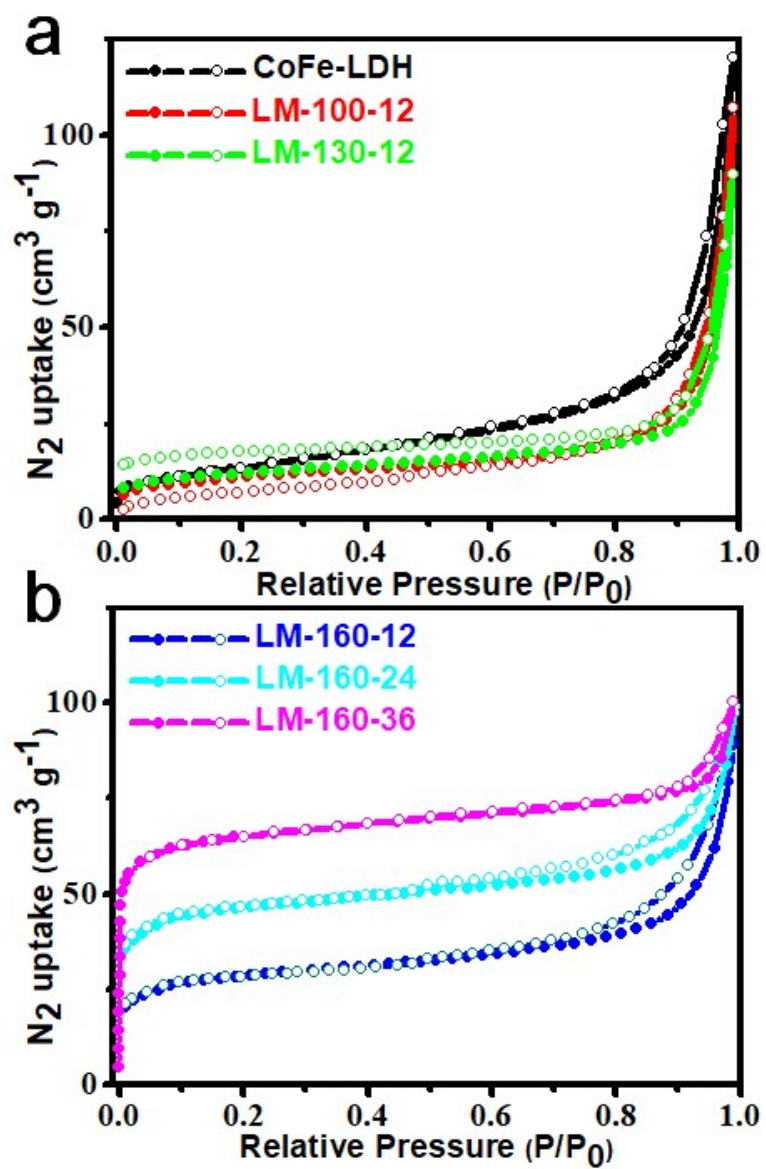
**Electrochemical Measurements.** A three-electrode glass cell with a platinum wire counter electrode, an Ag/AgCl reference electrode and glassy carbon (GC) working electrode on Autolab PGSTAT204 electrochemistry workstation was carried out to test electrochemical performance. The measured potentials versus the reversible hydrogen electrode (RHE) were converted according to the equation:  $E_{\text{RHE}} = E_{\text{Ag/AgCl}} + 0.197 + 0.059 \times \text{pH}$ . For prepared work electrode, the specimens (5 mg), ethanol (490  $\mu\text{L}$ ), deionized water (490  $\mu\text{L}$ ), and Nafion (20  $\mu\text{L}$ ) were mixed and dispersed by ultrasonic for 30 min. The working electrodes were obtained through dripping the catalyst ink (5  $\mu\text{L}$ ) on the glassy-carbon electrode with a loading of 0.35 mg cm<sup>-2</sup>. Linear sweep voltammetry (LSV) were measured at a scan rate of 5 mV s<sup>-1</sup>. The potential in the LSV polarization curves were corrected for iR compensate. The electrochemical active surface areas (ECSA) were evaluated by measuring the double-layer capacitance (C<sub>dl</sub>) via cyclic voltammograms (CV) at different scan rates. The CV was measured in the potential range from 1.22 to 1.32 V vs RHE at different scan rate. Electrochemical

impedance spectroscopy (EIS) was measured with 5 mV amplitude in a frequency range from 100000 to 0.1 Hz at 1.50 V vs RHE.

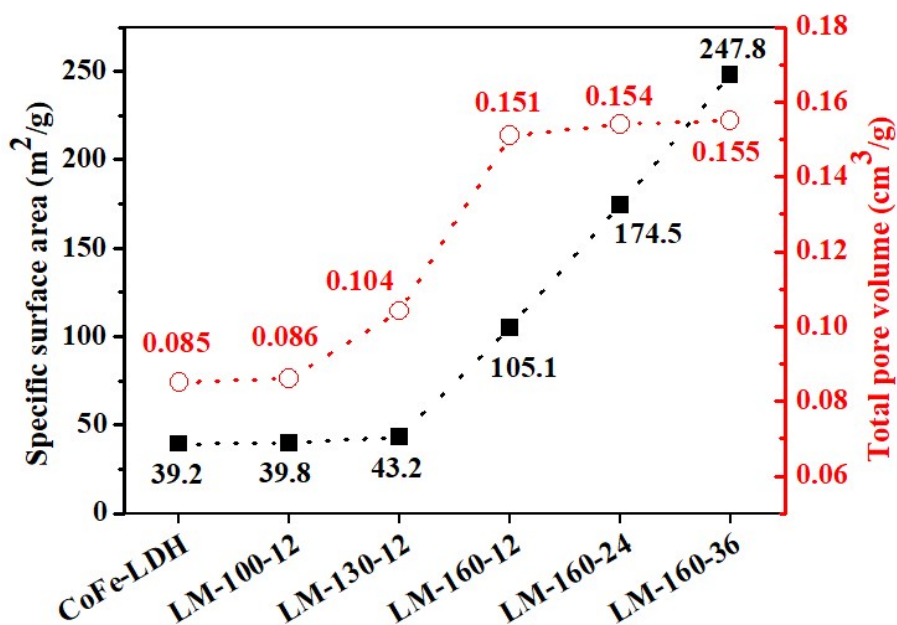
**Figures and Tables**



**Fig. S1** PXR D patterns of the prepared CoFe-LDH, LM-100-12 and LM-130-12 (a); LM-160-12, LM-160-24 and LM-160-36 (b).

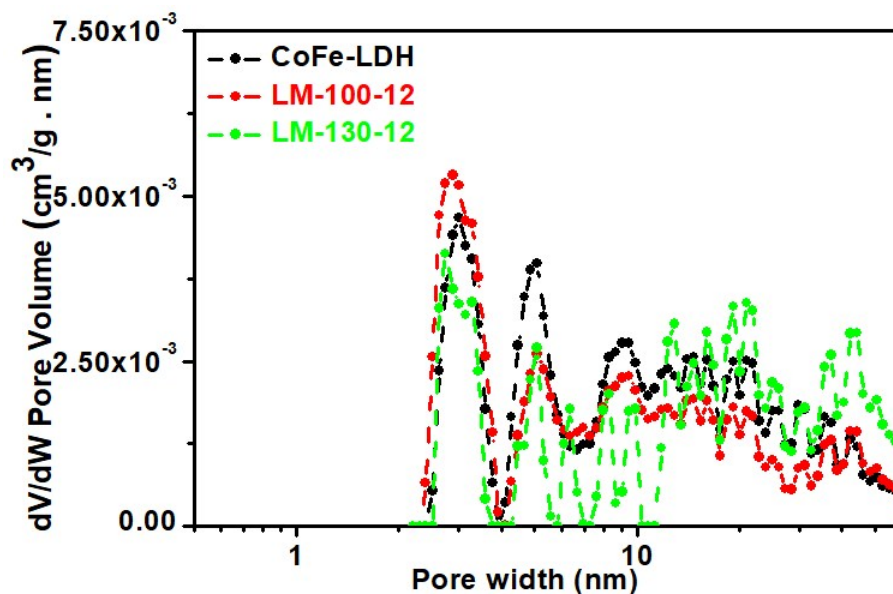


**Fig. S2** N<sub>2</sub>-adsorption/desorption isotherms of the prepared CoFe-LDH, LM-100-12 and LM-130-12 (a); LM-160-12, LM-160-24 and LM-160-36 (b).

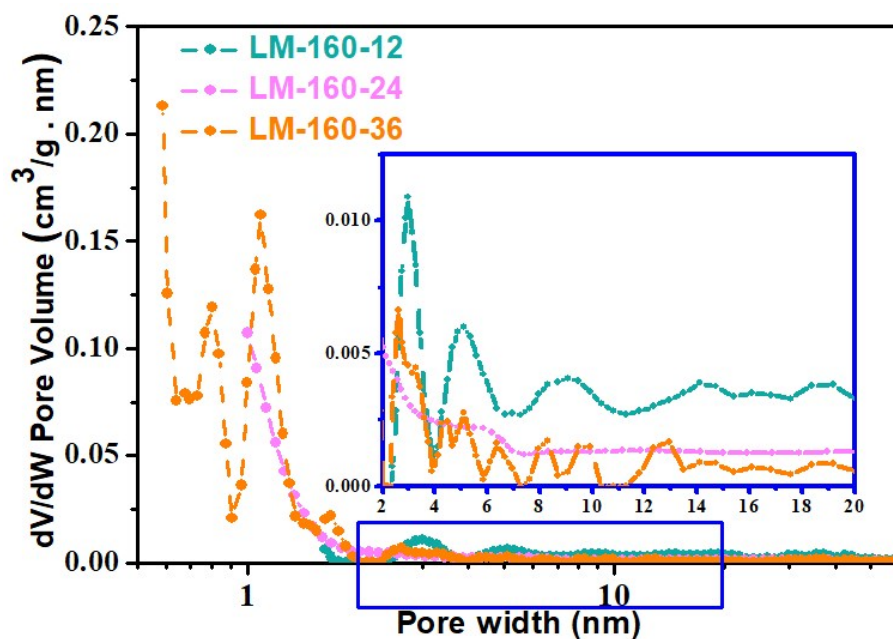


**Fig. S3** BET surface areas and total pore volume for all samples.

By combining PXRD and N<sub>2</sub>-adsorption/desorption results, it is obvious the successful transformation requires appropriate conversion temperature and time. Prepared MOFs with ligand-assisted procedure show bigger specific surface and total pore volume, compared with precursor CoFe-LDH.



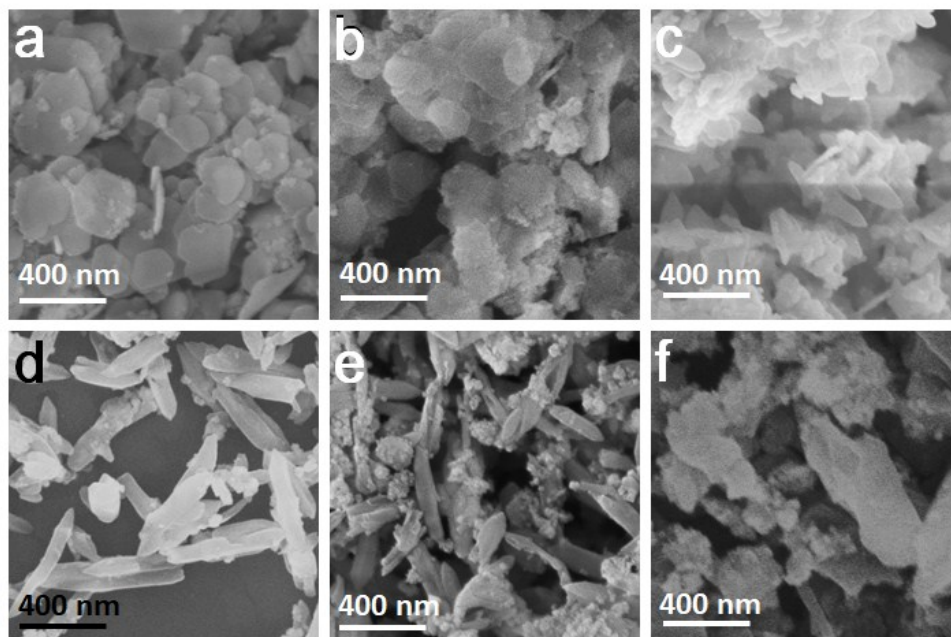
**Fig. S4** Pore size distribution was calculated by nonlocal density functional theory (NLDFT) for CoFe-LDH, LM-100-12 and LM-130-12.



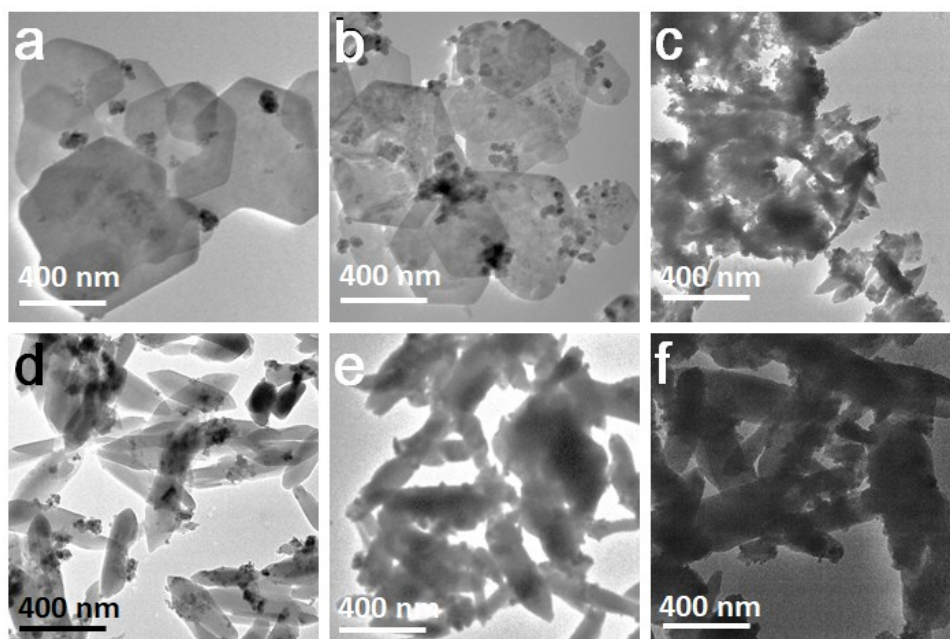
**Fig. S5** Pore size distribution was calculated by nonlocal density functional theory (NLDFT) for LM-160-12, LM-160-24 and LM-160-36.

Fig. S4-5 showed that the mesoporous distribution of LM-160-12 was the largest compared with other samples. And microporous distribution dominated the LM-160-36, which confirmed the existence of MIL-88B. Based on pore size distribution and PXRD results, the LM-160-36 was confirmed as a mixture of two kinds of MOFs correspondingly.





**Fig. S6** SEM images of all samples. (a) CoFe-LDH, (b) LM-100-12, (c) LM-130-12, (d) LM-160-12, (e) LM-160-24 and (f) LM-160-36.



**Fig. S7** TEM images of all samples. (a) CoFe-LDH, (b) LM-100-12, (c) LM-130-12, (d) LM-160-12, (e) LM-160-24 and (f) LM-160-36.

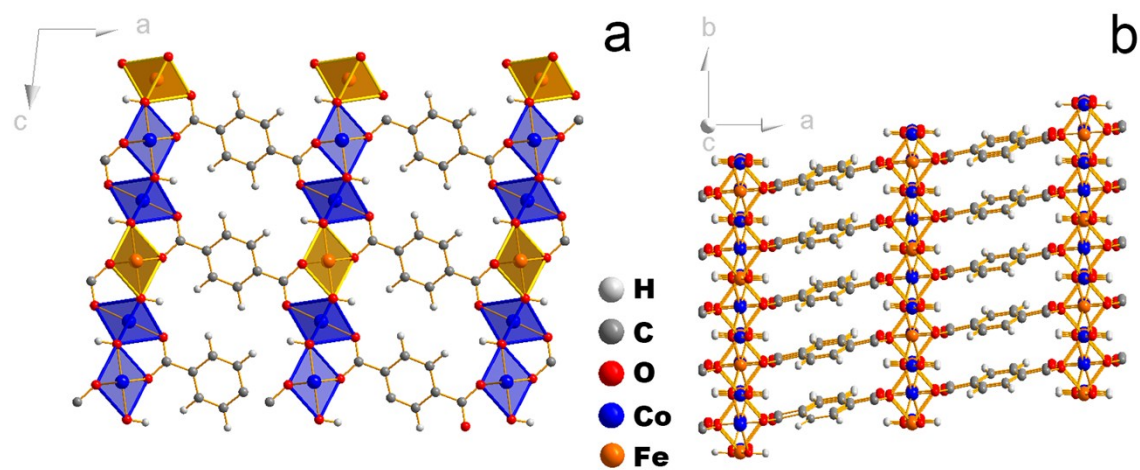


**Fig. S8** Crystal structure diagram of CoFe-2D-MOF derived from Ni-MOF with the known crystal structure of  $[\text{Ni}_3(\text{OH})_2(1,4\text{-BDC})_2(\text{H}_2\text{O})_4]\cdot 2\text{H}_2\text{O}$ .

**Table S1** Comparisons of WOR activity of cobalt-based electrocatalysts performed in 1.0 M KOH electrolyte.

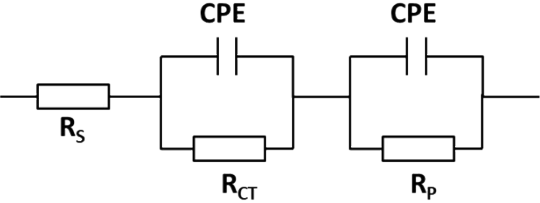
WOR catalyst	Metal species	Overpotential at 10 mA cm <sup>-2</sup> (mV)	Tafel slope (mV dec <sup>-1</sup> )	Stability (hour)	Reference
<b>LM-160-12</b>	<b>Co, Fe</b>	<b>274</b>	<b>46.7</b>	<b>70</b>	<b>This work</b>
<b>LM-160-24</b>	<b>Co, Fe</b>	<b>300</b>	<b>46.9</b>	<b>N/A</b>	<b>This work</b>
A <sub>2.7</sub> B-MOF-FeCo <sub>1.6</sub>	Co, Fe	288	39	10	<i>Adv. Energy Mater.</i> <b>2018</b> , 1801564
Co@NC-3/1	Co	380	90	10	<i>Adv. Energy Mater.</i> <b>2018</b> , 8, 1702048
Mn-CoP	Co, Mn	290	76	20	<i>Dalton Trans.</i> <b>2018</b> , 47, 14679–14685
Phy-Co <sup>2+</sup> /Fe <sup>3+</sup>	Co, Fe	301	46.38	N/A	<i>J. Mater. Chem. A</i> , <b>2018</b> , 6, 805-810
Co-LDHNS- II	Co	340	56	N/A	<i>J. Mater. Chem. A</i> , <b>2018</b> , 6, 5999-6006
d-Co-LDHs-1	Co	289	55.1	N/A	<i>J. Mater. Chem. A</i> , <b>2018</b> , 6, 4636–4641
exfoliated Co(OH) <sub>2</sub> nanosheets	Co	292	N/A	N/A	<i>Adv. Energy Mater.</i> <b>2018</b> , 8, 1702965
MnO@Co-N/C	Mn, Co	412	N/A	N/A	<i>J. Mater. Chem. A</i> , <b>2018</b> , 6, 9716–9722
Mn <sub>3-x</sub> Co <sub>x</sub> O	Mn, Co	460	31	10	<i>RSC Adv.</i> , <b>2016</b> , 6, 2019–2023
MnCo <sub>2</sub> O <sub>x</sub>	Mn, Co	410	84	20	<i>J. Am. Chem. Soc.</i> <b>2014</b> , 136, 16481.
CoCo LDH	Co	393	59	10	<i>Nat. Commun.</i> <b>2014</b> , 5, 4477

CoO <sub>x</sub> @CN	Co	385	N/A	2	<i>J. Am. Chem. Soc.</i> <b>2015</b> , 137, 2688.
Co-P/NC	Co	319	52	24	<i>Chem. Mater.</i> <b>2015</b> , 27, 7636
Co-P films	Co	345	47	N/A	<i>Angew. Chem. Int. Ed.</i> <b>2015</b> , 127, 6349
Zn <sub>x</sub> Co <sub>3-x</sub> O <sub>4</sub> yolk-shell polyhedron	Zn, Co	337	59.3	N/A	<i>ACS Appl. Mater. Interfaces</i> <b>2017</b> , 9, 31777
Zn-doped CoSe <sub>2</sub> /CFC	Zn, Co	356	88	10	<i>ACS Appl. Mater. Interfaces</i> <b>2016</b> , 8, 26902
Ni-Co Nanowire	Ni, Co	302	43.6	20	<i>Adv. Energy Mater.</i> <b>2017</b> , 7, 1601492
Mn-Co oxyphosphide	Mn, Co	320	52	88	<i>Angew. Chem. Int. Ed.</i> <b>2017</b> , 56, 2386–2389
Ag-CoSe <sub>2</sub>	Co, Ag	320	56	N/A	<i>Angew. Chem. Int. Ed.</i> <b>2017</b> , 56, 328–332
Fe-Co-P	Fe, Co	252	33	N/A	<i>ACS Nano</i> <b>2018</b> , 12, 158
Co <sub>3</sub> S <sub>4</sub> @MoS <sub>2</sub>	Co, Mo	280	43	N/A	<i>Nano Energy</i> , <b>2018</b> , 47, 494
Ni <sub>0.6</sub> Co <sub>1.4</sub> P	Ni, Co	300	80	100	<i>Adv. Funct. Mater.</i> <b>2018</b> , 28, 1706008
Co/Co <sub>3</sub> O <sub>4</sub> @PGS	Co	350	76.1	N/A	<i>Adv. Energy Mater.</i> <b>2018</b> , 8, 1702900
Zn <sub>0.1</sub> Co <sub>0.9</sub> Se <sub>2</sub>	Co, Zn	340	43.2	N/A	<i>J. Mater. Chem. A</i> , <b>2017</b> , 5, 17982
NiCo-UMOFNs	Ni, Co	250	42	200	<i>Nat. Energy</i> , <b>2016</b> , 1, 16184.
LDH FeCo	Fe, Co	330	85	N/A	<i>Science</i> , <b>2016</b> , 352, 333
CoMn LDH	Co, Mn	324	43	10	<i>J. Am. Chem. Soc.</i> <b>2014</b> , 136, 16481

**Table S2** Comparisons of WOR activity of pristine MOFs performed in various electrolytes.

WOR catalyst	Metal species	Overpotential at 10 mA cm <sup>-2</sup> (mV)	Tafel slope (mV dec <sup>-1</sup> )	Testing condition	Reference
<b>LM-160-12</b>	<b>Co, Fe</b>	<b>274</b>	<b>46.7</b>	<b>1.0 M KOH</b>	<b>This work</b>
<b>LM-160-24</b>	<b>Co, Fe</b>	<b>300</b>	<b>46.9</b>	<b>1.0 M KOH</b>	<b>This work</b>
A <sub>2.7</sub> B-MOF-FeCo <sub>1.6</sub>	Co, Fe	288	39	1.0 M KOH	<i>Adv. Energy Mater.</i> <b>2018</b> , 1801564
Co/MIL-101(Cr)	Co, Cr	850	130	1.0 M KOH	<i>Int. J. Hydrogen Energy</i> <b>2015</b> , 31, 9713-9722
Pb-TCPP	Pb	470	106.2	1.0 M KOH	<i>Dalton Trans.</i> <b>2016</b> , 45, 61-65
NH <sub>2</sub> -MIL-53(Fe)	Fe	390	72.9	1.0 M KOH	<i>Nanoscale</i> <b>2016</b> , 8, 1033-1039
MAF-X27-Cl	Co	292	N/A	1.0 M KOH	<i>J. Am. Chem. Soc.</i> <b>2016</b> , 138, 8336–8339
UTSA-16	Co	408	N/A	1.0 M KOH	<i>ACS Appl. Mater. Interfaces</i> <b>2017</b> , 9, 7193–7201
CoCd-BNN	Co, Cd	390	110	1.0 M KOH	<i>ACS Appl. Mater. Interfaces</i> <b>2017</b> , 9, 37548–375
Fe/Ni <sub>2.4</sub> -MIL-53	Ni, Fe	244	48.7	1.0 M KOH	<i>Angew. Chem.</i> <b>2018</b> , 130, 1906–1910
Ti <sub>3</sub> C <sub>2</sub> T <sub>x</sub> -CoBDC	Co, Ti	410	48.2	1.0 M KOH	<i>ACS Nano</i> <b>2017</b> , 11, 5800–5807
2D CoZIF-9(III) sheets	Co	380	55	1.0 M KOH	<i>Adv. Sci.</i> <b>2018</b> , 5, 1801029
CoFe-MOF-OH	Co, Fe	265	44	1.0 M KOH	<i>ACS Catal.</i> <b>2019</b> , 9, 7356–7364

**Table S3** The equivalent circuit diagram and comparisons of  $R_s$ ,  $R_{ct}$ ,  $R_p$  and  $CPE$  for prepared electrocatalysts.



$R_s$  solution resistance  
 $R_{ct}$  electron transfer resistance  
 $R_p$  surface porosity resistance  
 $CPE$  constant phase element

Z/ohm	CoFe-LDH	LM-100-12	LM-130-12	LM-160-12	LM-160-24	LM-160-36
$R_s$	9.59	8.01	8.64	8.95	9.20	8.56
$R_{CT}$	97.2	92.0	74.2	47.8	49.8	42.0
$R_p$	39.6	13.4	5.4	3.4	9.5	6.4

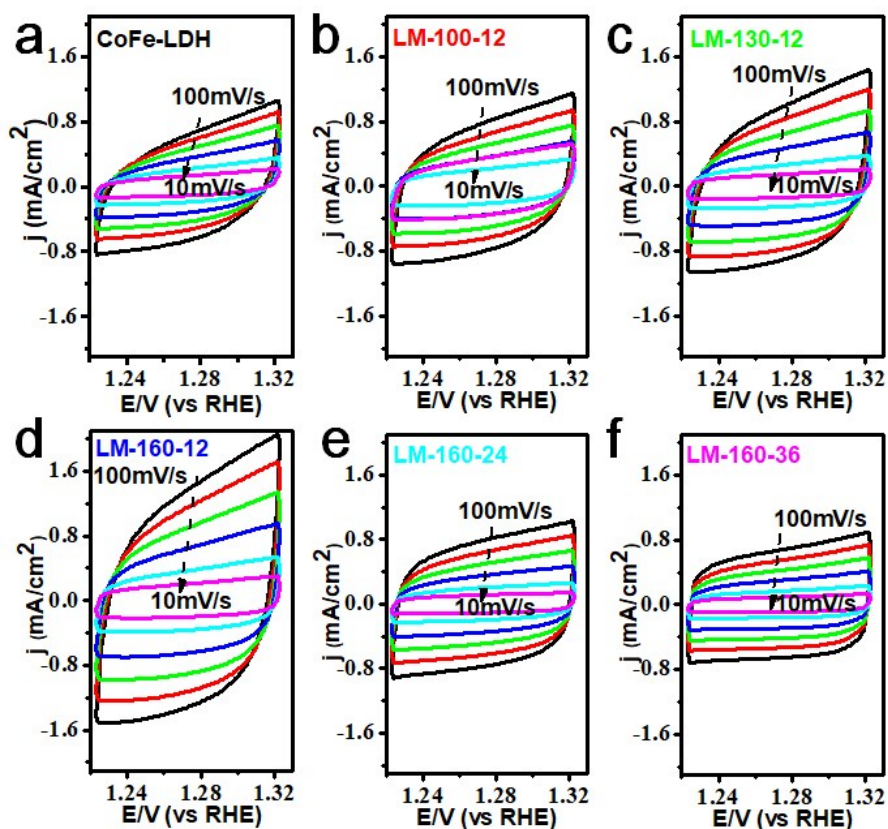


**Fig. S9** (a-f) CV plots of all prepared samples.

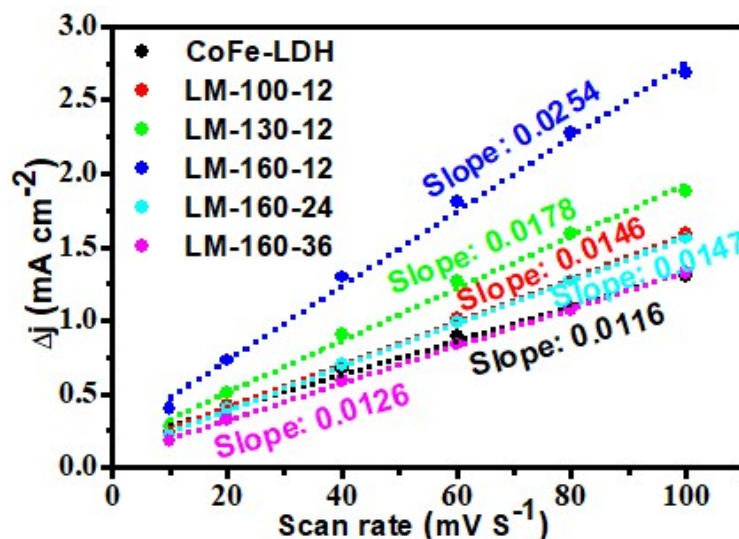


**Fig. S10** Capacitive currents as a function of the scan rate to give the double-layer capacitance for all samples.

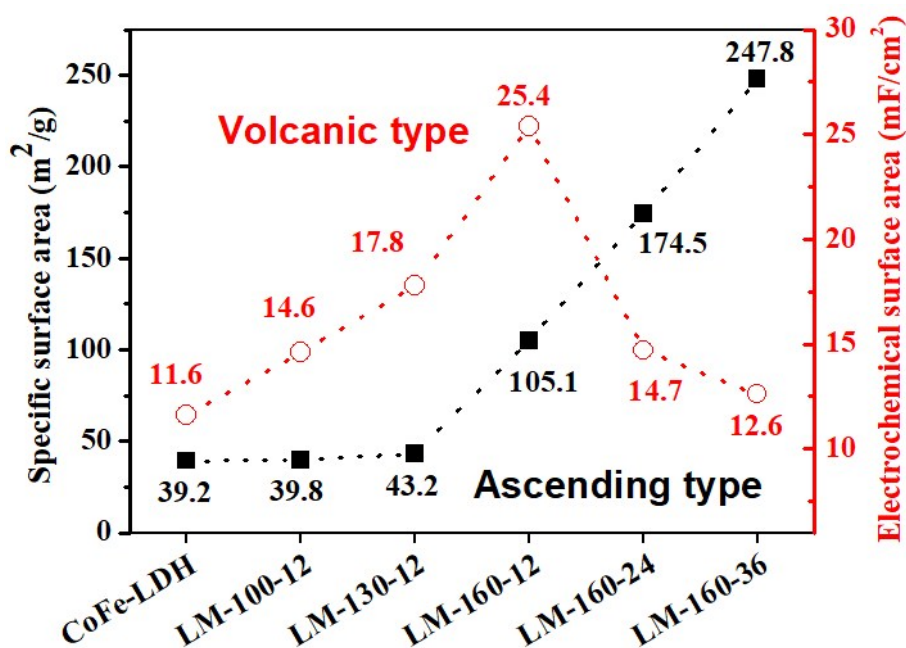


**Fig. S11** BET surface areas versus ESCA for all samples.

As shown in Fig. S9, it was clear that ESCA is not simply up to the BET specific surface in our case. BET is calculated based on microporous adsorption, but a large number of mesoporous distributions improved the electrochemical active area in our case, which emphasized the importance of 2D morphology.



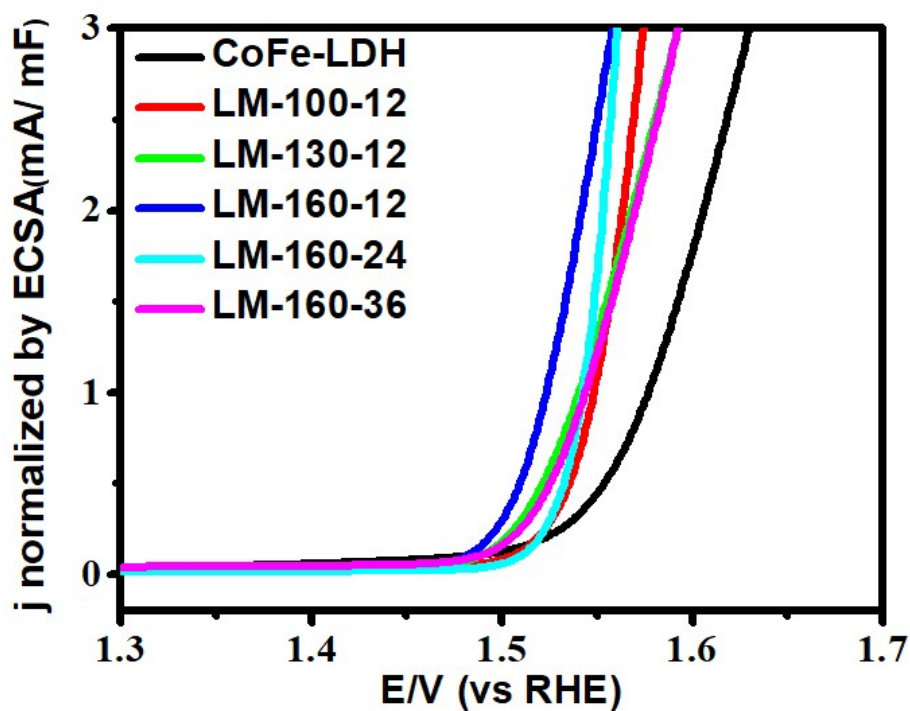


Fig. S12 The LSV curves normalized by ECSA for all samples.

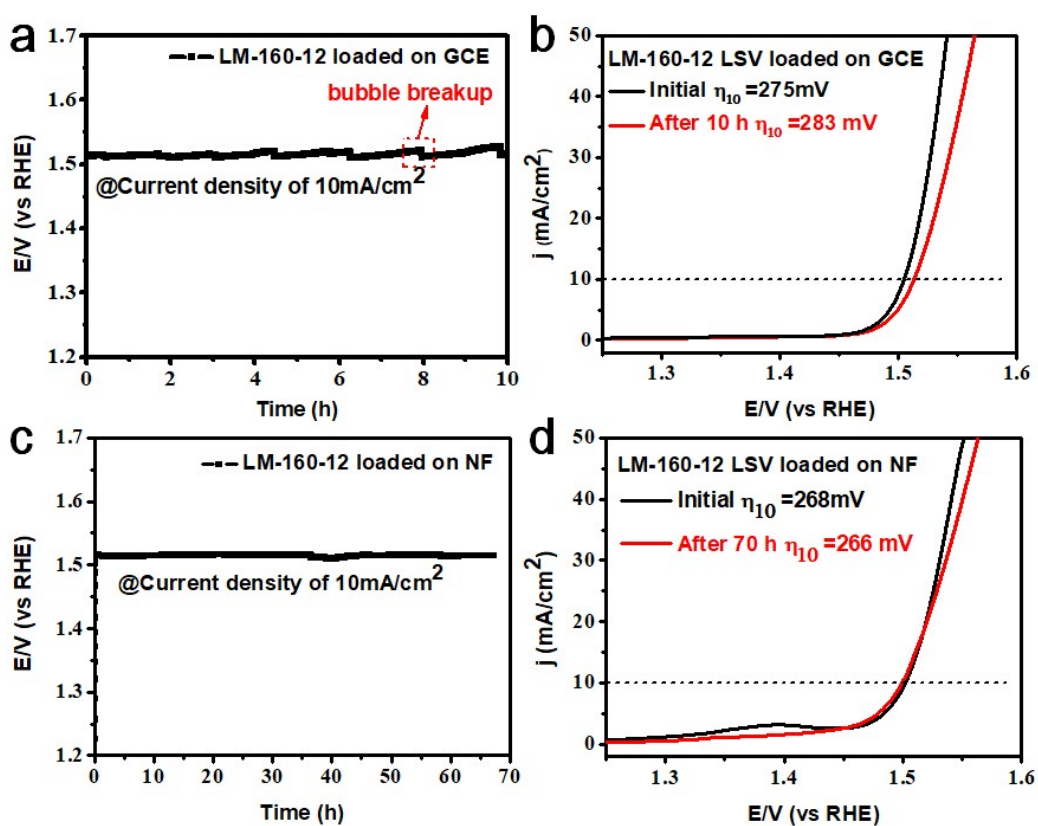
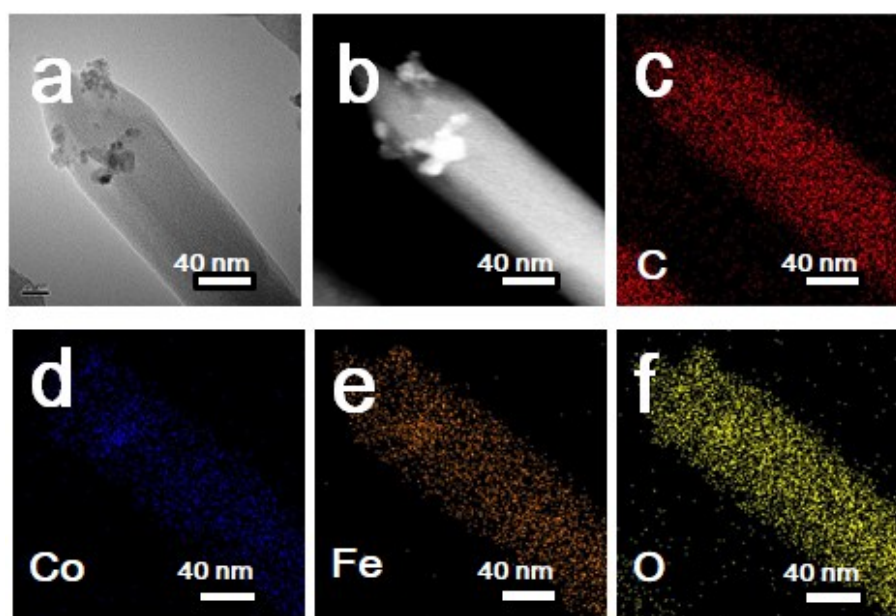


Fig. S13 Electrocatalytic stability test. Chronopotentiometry curves of LM-160-12



loaded on (a) GCE for 10 h and (c) NF for 70 h at  $10 \text{ mA cm}^{-2}$  in  $1.0 \text{ M KOH}$ . Comparison of LSV plots between initial state and after long-term WOR, loaded on (b) GCE for 10 h and (d) NF for 70 h. Electrochemical stability test. Both the glassy carbon and nickel foam electrode with a loading of  $0.35 \text{ mg cm}^{-2}$  were conducted at the same current density  $10 \text{ mA cm}^{-2}$ , but the area of glassy carbon electrode is about  $0.07 \text{ cm}^2$  and nickel foam electrode is about  $1 \text{ cm}^2$ .



**Fig. S14** Morphology characterization after 70 h WOR process. TEM (a), HAADF-STEM (b) and EDXS mapping images for C (c), Co (d), Fe (e) and O (f) of LM-160-12 after 70 h WOR process.

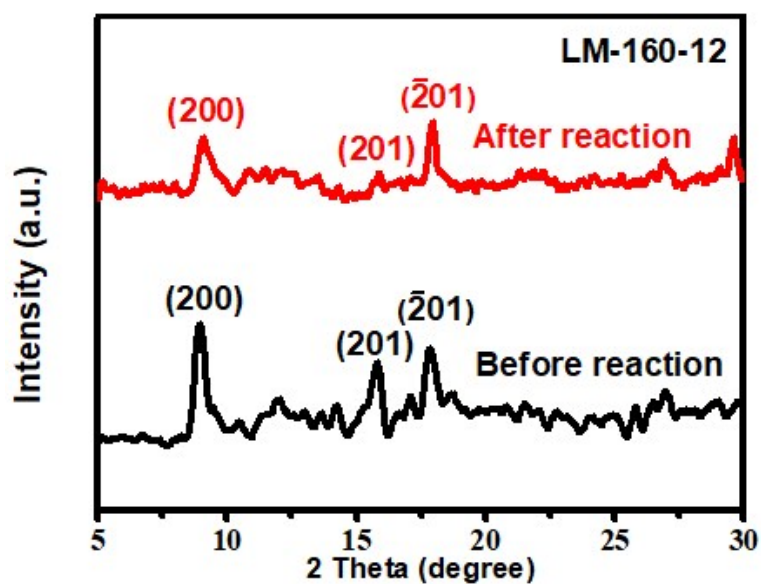


Fig. S15 PXR D patterns of LM-160-12 before and after 70 h WOR process.

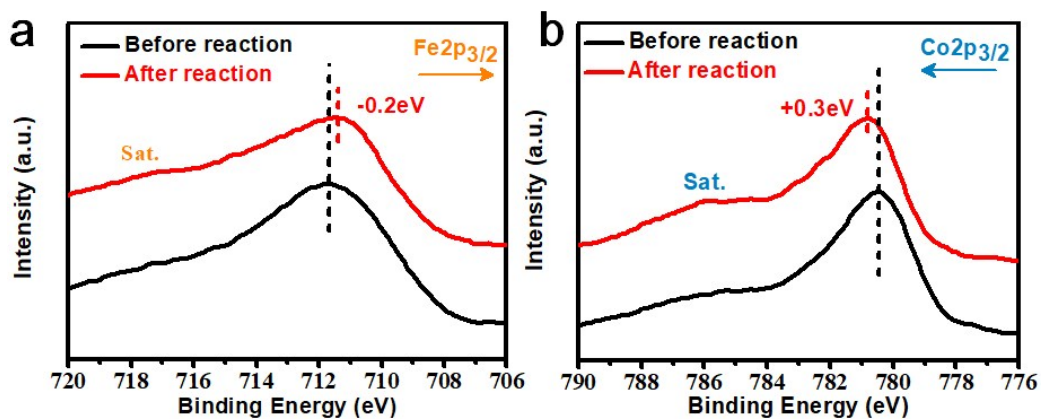
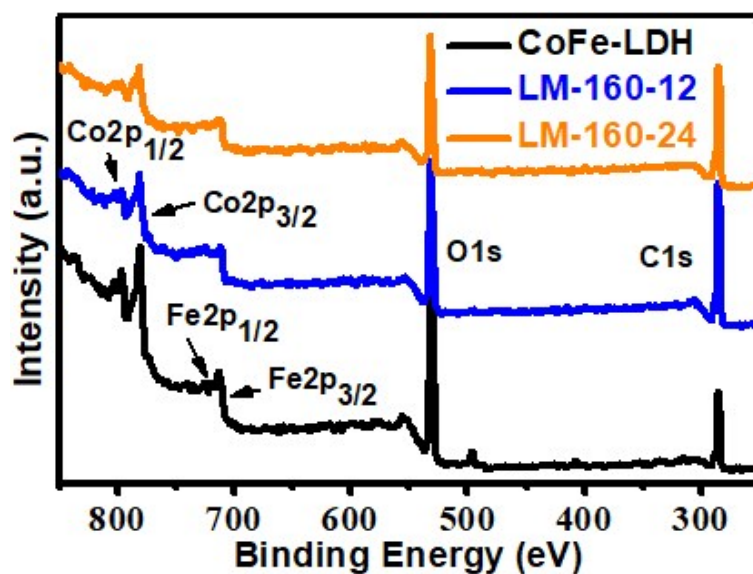
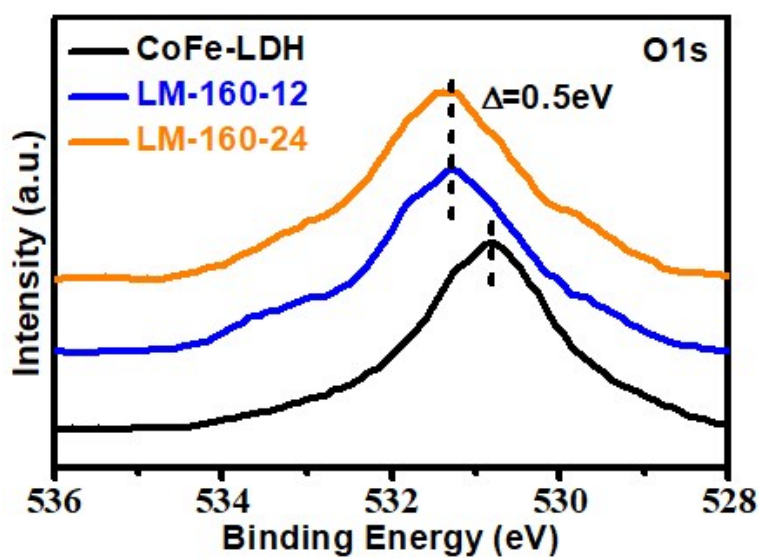


Fig. S16 Fe  $2p_{3/2}$  (a) and Co  $2p_{3/2}$  (b) XPS of LM-160-12 before and after 70 h electrocatalytic test at  $10 \text{ mA cm}^{-2}$ .



**Fig. S17** Full range XPS spectra of precursor CoFe-LDH, LM-160-12 and LM-160-24.



**Fig. S18** O 1s high resolution XPS spectra of precursor CoFe-LDH, LM-160-12 and LM-160-24.

**Table S4** The chemical composition and molar ratio of Co/Fe detected by XPS.

Samples	C/molar %	O/molar %	Co/molar %	Fe/molar %	Molar ratio Co/Fe
CoFe-LDH	40.9	42.4	11.4	5.4	2.1
LM-160-12	62.8	27.7	6.3	3.2	2.0
LM-160-24	63.7	28.2	5.0	3.1	1.6

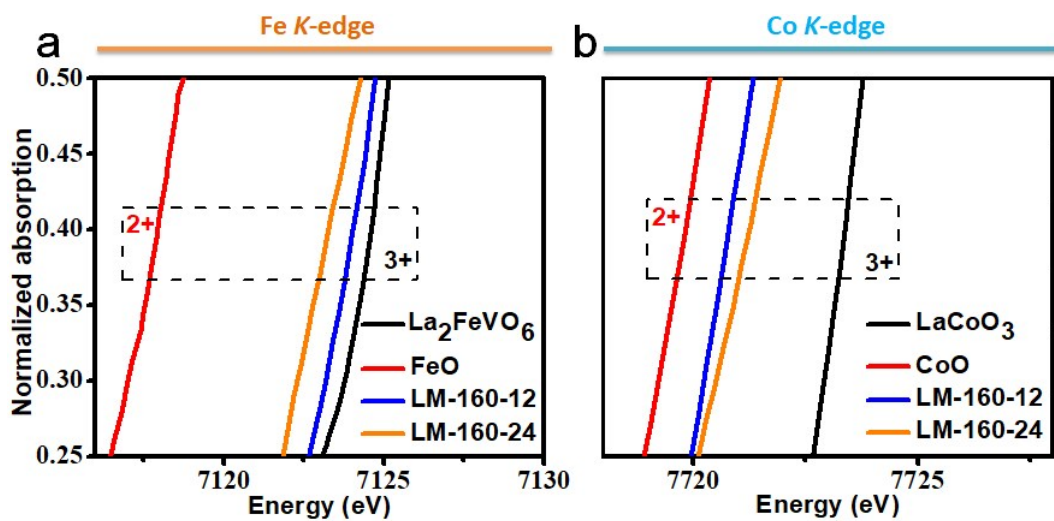


**Fig. S19** Expanded near edge spectra of LM-160-12 and LM-160-24. (a) Fe K-edge and (b) Co K-edge of LM-160-12 and LM-160-24.